Scientific Research Publishing

Open Journal of Applied Sciences, 2025, 15(4), 919-937
https://www.scirp.org/journal/ojapps
ISSN Online: 2165-3925
ISSN Print: 2165-3917

Dynamic Analysis of Nose Landing Gear Shimmy Considering Strut Height and Experiment on the Test Platform

Xiangzhi Xiao, Yanying Zhao, Hao Wu, Guisheng Zhu

School of Aircraft Engineering, Nanchang Hangkong University, Nanchang, China
Email: 1367221491@qq.com

How to cite this paper: Xiao, X.Z., Zhao, Y.Y., Wu, H. and Zhu, G.S. (2025) Dynamic Analysis of Nose Landing Gear Shimmy Considering Strut Height and Experiment on the Test Platform. *Open Journal of Applied Sciences*, **15**, 919-937.
https://doi.org/10.4236/ojapps.2025.154062

Received: March 18, 2025
Accepted: April 7, 2025
Published: April 10, 2025

Abstract

This study investigates the influence of strut height on the shimmy stability of aircraft nose landing gear through both theoretical modeling and experimental validation. A nonlinear dynamic model incorporating strut height is established to derive analytical expressions for the critical shimmy speed. The effects of key structural parameters, including lateral bending stiffness, torsional stiffness, damping, diagonal brace positioning, and shimmy damper installation height, are systematically analyzed. The results indicate that increasing strut height significantly reduces lateral bending stiffness and damping, leading to a lower critical shimmy speed and reduced stability. To validate the theoretical findings, a nose landing gear shimmy test platform was developed, and high-precision laser vibrometry was used to capture the dynamic responses under different taxiing speeds. The experimental results align closely with theoretical predictions, confirming the accuracy of the model and providing quantitative insights into the relationship between strut height and shimmy stability. This research offers valuable theoretical guidance and engineering recommendations for optimizing landing gear designs, particularly for aircraft with high-strut configurations.

Keywords

Nose Landing Gear, Strut Height, Shimmy, Stability, Experimental Validation

1. Introduction

Landing gear shimmy is a self-excited instability phenomenon caused by coupled multi-degree-of-freedom vibrations. It typically occurs within a frequency range of 5 - 30 Hz, with oscillation amplitudes generally below 20˚ [1].

As studies progressed, researchers expanded model complexity and parameter

analysis. Liu Shengli *et al.* [2] [3] experimentally demonstrated that weak local stiffness at the landing gear-airframe connection significantly reduces the system's stability region, providing critical insights for structural optimization. Building on this, Thota *et al.* [4] developed a three-degree-of-freedom nonlinear model incorporating strut lateral bending, torsion, and tire deformation, successfully identifying bifurcation characteristics and stability boundaries. Further refinement by Thota *et al.* [5] revealed that strut longitudinal bending has negligible influence on stability, simplifying engineering models. posing risks to both passenger comfort and flight safety. To unravel this complex dynamic behavior, Somieski [6] pioneered a two-degree-of-freedom model for nose landing gear shimmy, systematically analyzing the coupling effects of key parameters such as tire lateral stiffness, damping coefficients, shock absorber damping, and strut elasticity. This foundational work laid the theoretical groundwork for subsequent research.

Recent research has focused on refining strut torsional dynamics. Rahmani *et al.* [7] decomposed strut torsion into three components: lower strut rotation, upper strut rotation, and shimmy damper rotation. Their parametric analysis confirmed that reducing lower strut stiffness while increasing damper damping significantly enhances stability—offering key design principles for shimmy suppression systems.

In the mid-20th century, significant breakthroughs were made in the study of shimmy in nose landing gears, leading to the emergence of two representative theoretical models: the point-contact theory of tires and the string theory. Based on different assumptions regarding tire dynamic characteristics, Moreland *et al.* [8] and Smiley *et al.* [9] proposed these two distinct theoretical models, respectively. The reliability of these models was confirmed through extensive theoretical derivations and experimental data, and they have since been widely applied and recognized in practical engineering applications. Boeckh [10] measured experimental data for four different types of tires and calculated the rotational inertia of the tires around the vertical axis, thereby validating the effectiveness of the string model proposed by Von Schlippe *et al.* [11].

As a structure designed to withstand impact loads and provide damping during aircraft takeoff and landing, the landing gear system ensures the safety and stability of aircraft during takeoff, landing, and ground taxiing. Statistical data indicate that approximately one-third of aircraft accidents are directly or indirectly related to failures in the landing gear system.

The landing gear system, as a structure designed to withstand impact loads and provide damping during aircraft takeoff and landing, ensures the safety and stability of aircraft during takeoff, landing, and ground taxiing. Statistical data indicate that approximately one-third of aviation accidents are directly or indirectly related to landing gear system failures [12]-[19].

With the continuous increase in modern aircraft weight and takeoff speeds, higher demands are placed on the design performance of landing gears. Particularly during the landing phase, the majority of the impact energy is absorbed by the damping and shock-absorption mechanisms of the main landing gear, while the air-

frame structure absorbs only a small portion. Therefore, the reliability of the landing gear is directly linked to the safety of aircraft during takeoff and landing.

This design improves adaptability to various runway conditions and reduces the risk of engine foreign object inhalation. However, greater strut height also notably affects the lateral bending stiffness and damping characteristics of the landing gear, thereby impacting shimmy stability. With the increasing complexity of aircraft design and higher performance requirements for landing gear, optimizing strut height has become a critical issue. Research indicates that increased strut height may lead to bifurcation phenomena in landing gear shimmy, triggering instability that severely compromises aircraft safety and passenger comfort [17] [20]-[26]. Given the significant impact of strut height on landing gear stability, this study establishes a dynamic shimmy analysis model for nose landing gear that incorporates strut height. Through quantitative analysis of the effects of strut height and slenderness ratio on lateral bending stiffness and torsional stiffness, the study investigates their combined influence on shimmy critical speed and stability. Additionally, the effects of diagonal brace installation position and shimmy damper damping on shimmy critical speed and frequency are analyzed.

2. Modeling and Analysis

2.1. Nose Landing Gear Dynamic Model Considering Strut Height

The nose landing gear is modeled as a simplified mechanical system incorporating the strut's lateral bending and torsional characteristics.

In Figure 1, L_g represents the height of the landing gear strut, and H_1 denotes the distance from the installation point of the diagonal strut and shimmy damper to the landing gear mounting point. The shimmy damper is simplified as a massless spring-damper system with lateral stiffness K_1 and damping C_1. The nose landing gear is simplified as a mass-spring-damper system with mass m, lateral bending stiffness K_s, and damping C_s.

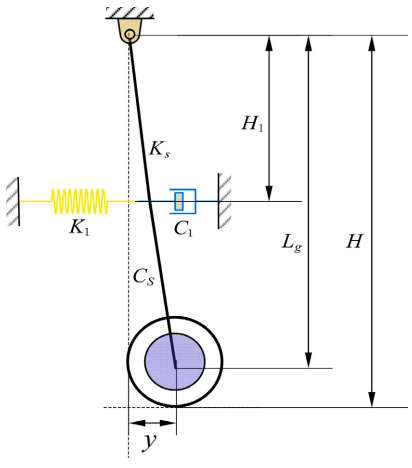

Figure 1. Front view of simplified mechanical model of nose landing gear considering diagonal strut and pendulum damper.

Figure 2 shows the top view of the dynamic model for the landing gear system shimmy analysis. Below, the calculation process for the parameters in the shimmy dynamic equations is introduced.

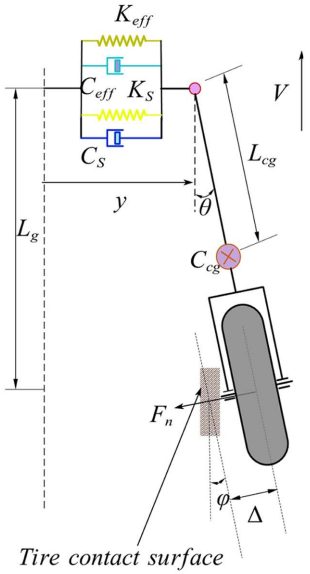

Figure 2. Top view of dynamic model for landing gear system shimmy analysis.

Assuming that the angular displacement at each point in the lateral bending of the strut is equal, the lateral bending stiffness and damping coefficients of the diagonal strut are derived based on the moment equilibrium equation and energy conservation theorem:

$$K_{eff} = K_1\left(\frac{H_1}{L_g}\right)^2, \quad C_{eff} = C_1\left(\frac{H_1}{L_g}\right)^2 \tag{1}$$

The equivalent lateral bending stiffness and damping coefficient of the strut in the nose landing gear system are K_{s1} and C_{s1}, respectively:

$$K_{s1} = K_s + K_{eff}, \quad C_{s1} = C_s + C_{eff} \tag{2}$$

Considering the presence of a rake angle δ, the equivalent stability margin L_{eff} from the wheel center to the strut axis is calculated as follows:

$$L_{eff} = L + R\tan(\delta) \tag{3}$$

Assuming the upper end of the nose landing gear strut is fixed, the system is analyzed with torsional freedom θ around the strut axis, lateral displacement y at the lower end of the strut, and lateral tire deformation Δ. The mass of the wheel and strut assembly is concentrated at their center of gravity, and the tire is assumed to experience no slip relative to the ground. The shimmy dynamic equations for the landing gear system are derived as follows:

$$m\ddot{y} + mL_{cg}\ddot{\theta} + C_{s1}\dot{y} + K_{s1}y + F_n = 0 \tag{4}$$

$$I\ddot{\theta} + mL_{cg}\ddot{y} + \left(C_{\theta} + C_{sh}\right)\dot{\theta} + K_{\theta}\theta + F_{n}L_{eff} + M_{n} = 0 \tag{5}$$

$$V\theta + \dot{y} + L_{eff}\dot{\theta} - \dot{\Delta} = 0 \tag{6}$$

Assuming the torsional angle θ is small, it can be approximated as $\sin\theta \cong 0$, $\cos\theta \cong 1$. The lateral force F_n acting on the nose landing gear tire can be expressed in terms of the lateral tire deformation Δ, denoted as $F_n = K_{\Delta}\Delta + C_{\Delta}\dot{\Delta}$ The aligning moment M_n can be expressed in terms of the tire torsional angle φ denoted as $M_n = K_{\varphi}\varphi + C_{\varphi}\dot{\varphi}$ where $\varphi \cong \Delta/\sigma$ are the lateral stiffness and torsional stiffness of the tire, respectively.

The nose landing gear strut is simplified as a cantilever beam fixed at one end and free at the other. Below, the lateral bending stiffness, torsional stiffness, lateral bending damping, and torsional damping coefficients of the strut are derived.

Lateral Bending Stiffness Coefficient:

The lateral bending stiffness coefficient of the landing gear strut describes its ability to resist bending deformation under lateral forces. For a circular cross-section beam, the lateral bending stiffness coefficient can be calculated using the following formula. By simplifying the nose landing gear strut as a cantilever beam fixed at one end, the lateral bending stiffness coefficient K_s is given by:

$$K_s = \frac{3E\pi d^4}{64L_g^3} \tag{7}$$

where E is the elastic modulus of the material, I is the moment of inertia of the cross-section, and L_g is the height of the strut. For a circular cross-section, the moment of inertia $I = \pi d^4/64$, where d is the diameter of the circular cross-section.

Lateral Bending Damping Coefficient:

The lateral bending damping coefficient of the landing gear strut describes its ability to dissipate energy during lateral vibrations. The damping coefficient is typically related to the material's damping properties. The lateral bending damping coefficient C_s is given by:

$$C_s = \zeta d^2\sqrt{\frac{3E\pi m}{4L_g^3}} \tag{8}$$

where ζ is the damping ratio and mm is the mass of the system. Substituting Equation (5) into this expression yields the lateral bending damping coefficient $C_s = 2\zeta\sqrt{K_s m}$.

Torsional Stiffness Coefficient:

The torsional stiffness coefficient of the landing gear strut describes its ability to resist torsional deformation under torque. For a cylindrical strut, the torsional stiffness coefficient K_{θ} is given by:

$$K_{\theta} = \frac{G\pi d^4}{32L_g} \tag{9}$$

where G is the shear modulus of the material, J is the polar moment of inertia of

the cross-section, and L_g is the height of the strut. For a circular cross-section, the polar moment of inertia $J = \pi d^4/32$ Substituting this into the formula yields the torsional stiffness coefficient.

Torsional Damping Coefficient:

The torsional damping coefficient of the landing gear strut describes its ability to dissipate energy during torsional vibrations. The damping coefficient is typically related to the material's damping properties. The torsional damping coefficient C_θ is given by:

$$C_\theta = \frac{\zeta \pi d^4}{16}\sqrt{\frac{G}{L_g}} \tag{10}$$

where ζ is the damping ratio, J is the polar moment of inertia, and K_θ is the torsional stiffness coefficient. Substituting the polar moment of inertia and torsional stiffness coefficient into this expression yields the torsional damping coefficient $C_\theta = 2\zeta\sqrt{K_\theta J}$.

2.2. Model Parameter

Table 1. Parameters of the nose landing gear.

Parameters	definition	value	unit
m	Mass of wheel and strut assembly	15	Kg
R	Wheel radius	0.1	m
δ	Rake angle	0.157	rad
ζ	Damping ratio	0.5	
H	Landing gear height	1	m
H_1	Distance from diagonal strut installation point to landing gear mounting point	0.3	m
L_g	Strut height	0.5	m
d	Strut diameter	0.1	m
L	Stability margin	0.07	m
L_{cg}	Distance from the center of mass of the wheel-strut assembly to the strut axis	0.01	m
I	Moment of inertia of the wheel-strut assembly about the strut axis	1	Kg·m²
K_s	Lateral bending stiffness of the strut	130,600	N/m
C_s	Lateral bending damping coefficient of the strut	0.012	N·m·s/rad
K_θ	Torsional stiffness of the strut	5400	N·m/rad
C_θ	Torsional damping coefficient of the strut	0.022	N·m·s/rad
K_1	Lateral stiffness of the diagonal strut	99,000	N/m
C_1	Lateral damping of the diagonal strut	0.01	N·m·s/rad
K_Δ	Lateral stiffness coefficient of the tire	112,000	N/m

Continued

C_{Δ}	Lateral damping coefficient of the tire	200	N·m·s/rad
K_{φ}	Torsional stiffness of the tire	1	m/rad
C_{φ}	Torsional damping coefficient of the tire	0.9	N·m·s/rad
σ	Relaxation height of the tire	0.22	m
C_{sh}	Shimmy damper damping	100	N·m·s/rad
V	Speed	0 - 100	m/s

3. Influence of Landing Gear Structural Parameters on Shimmy Stability and Time-Domain Response Analysis

To validate the reliability of the shimmy dynamic model of the landing gear, a time-domain simulation analysis is conducted with the following parameters: strut height L_g = 0.5 m, diagonal strut installation height H = 1 m, equivalent lateral bending stiff K_{s1} = 130,600 N/m, shimmy damper damping C_{sh} = 100 N·m·s/rad, and speed V = 60 m/s. Other parameters are consistent with those in Table 1.

First, taking a taxiing speed of 60 m/s as an example, the above parameters are substituted into the shimmy dynamic Equations (4)-(6) for simulation analysis. The time-history response curves of the strut torsional angle, strut lateral displacement, and tire lateral deformation are obtained, as shown in Figure 3.

From Figure 3, it can be observed that at a taxiing speed of 60 m/s, the strut torsional angle, strut lateral displacement, and tire lateral deformation all converge. Since the taxiing speed is below the critical shimmy speed of 67 m/s.

Next, taking a taxiing speed of 67 m/s as an example, the same parameters are substituted into the shimmy dynamic Equations (4)-(6) for simulation analysis. The time-history response curves of the strut torsional angle, strut lateral displacement, and tire lateral deformation are obtained, as shown in Figure 4.

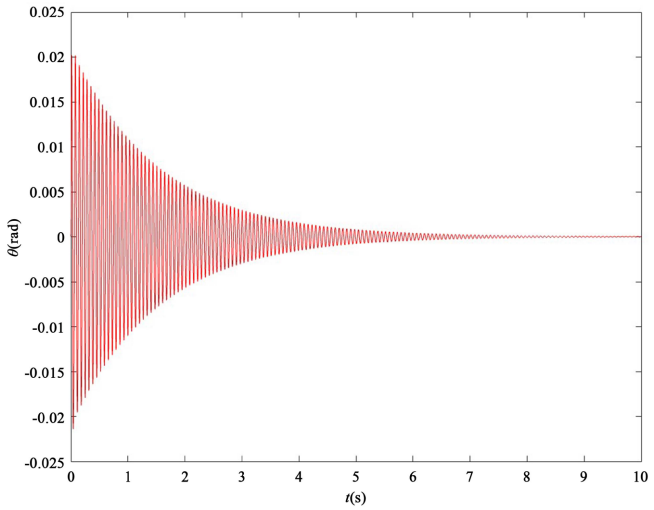

(a)

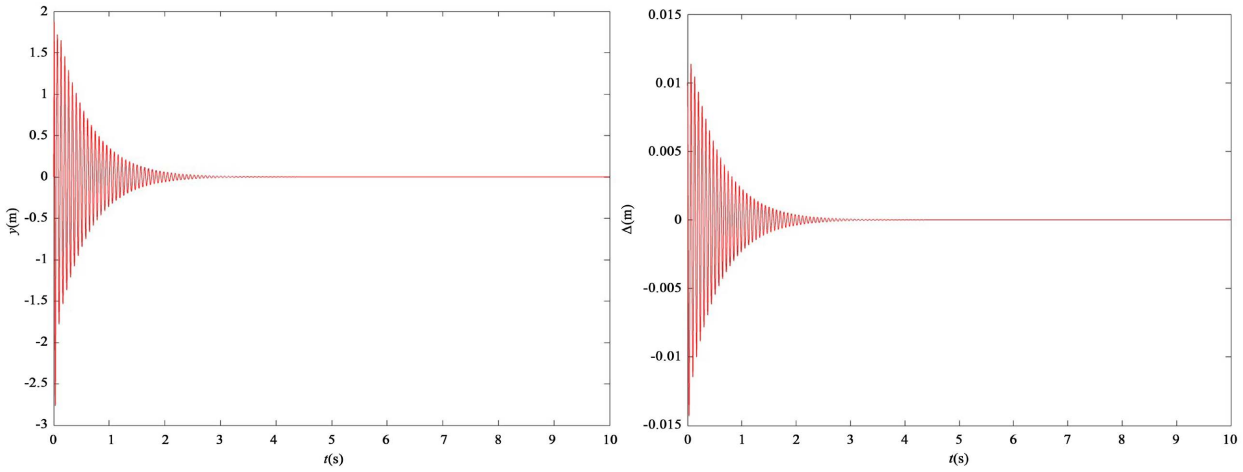

(b) (c)

Figure 3. Time history response curve at velocity 60 m/s (a) Angle of twist of the strut axis; (b) Lateral displacement of strut; (c) Lateral displacement of the wheel.

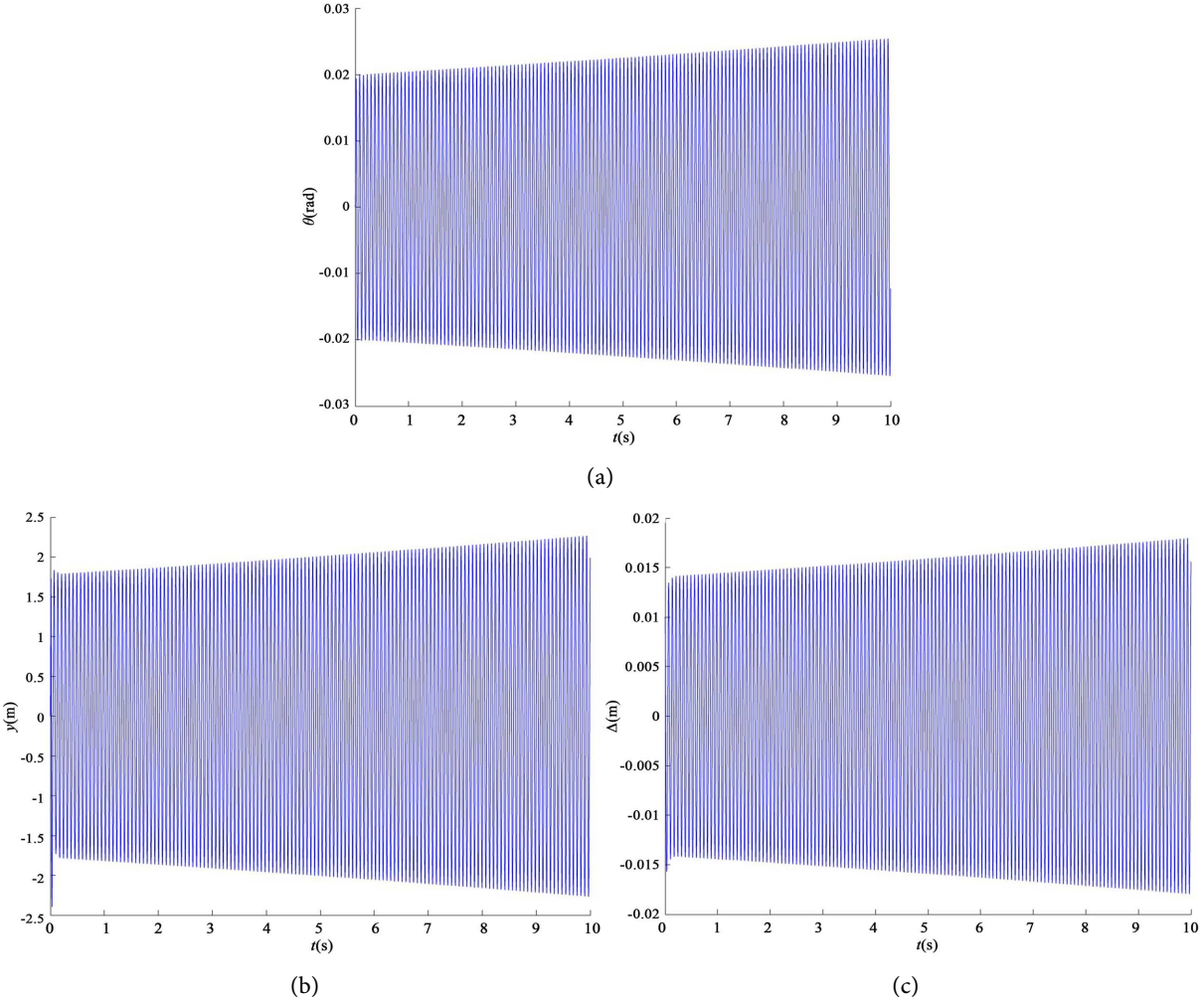

(a)

(b) (c)

Figure 4. Time history response curve at velocity 67 m/s. (a) Angle of twist of the strut axis; (b) Lateral displacement of strut; (c) Lateral displacement of the wheel.

4. Shimmy Test of the Landing Gear

To better analyze the dynamic characteristics of the landing gear, this study conducted shimmy experiments on the nose landing gear and collected experimental data. The primary objective of the experiments was to investigate the dynamic response of the nose landing gear under different taxiing speeds and periodic excitations, providing experimental data support for the analysis of landing gear shimmy stability.

By adjusting the rotational speed of the flywheel, the taxiing speed was controlled, and the dynamic response of the nose landing gear at different speeds was studied. Under low-speed conditions, the landing gear exhibited lower shimmy frequencies and amplitudes. At high taxiing speeds, as the shimmy speed of the system increased, the acceleration response also significantly increased. When the taxiing speed approached the critical speed, shimmy instability occurred, and the amplitude began to increase. However, after exceeding the critical speed, the nose landing gear tended to achieve dynamic stability. The experiments revealed that this instability in nose landing gear shimmy is closely related to factors such as the structural stiffness and damping of the strut.

Additionally, periodic excitations were introduced in the experiments to simulate the vibration response of the landing gear when encountering uneven ground or external loads. This helped to study the dynamic characteristics of the landing gear strut, such as displacement and acceleration, during shimmy. The response amplitude and frequency characteristics under resonant conditions were measured using a laser vibrometer and its analysis system. These results provide valuable experimental data references for the subsequent design of shimmy dampers for the nose landing gear.

4.1. Introduction to the Test Bench Equipment

The test utilized the PSVQTec3D ultra-low noise 3D scanning laser vibrometer. The QTec scanning laser vibrometer is one of the most advanced non-contact vibration measurement systems available today. This equipment is widely used in scientific research and development for determining vibration modes and characteristic frequencies in fields such as NVH (Noise, Vibration, and Harshness), acoustics, structural dynamics, ultrasonics, FEM (Finite Element Method) modal validation, and NDT (Non-Destructive Testing). The parameters of the single-wheel nose landing gear model used in the experiment are shown in **Figure 5**.

For each test condition, several different forward speeds of the nose landing gear were tested: 5 m/s, 10 m/s, 15 m/s, 20 m/s, 25 m/s, and 30 m/s. These speeds were selected because they cover the range at which shimmy commonly occurs in both heavy and light aircraft. The reported peak amplitude refers to the first positive peak, *i.e.*, the maximum amplitude after the impact [27]-[30].

4.2. Forward Speed Test on a Smooth Runway Surface

The first condition involves the forward speed test on a smooth runway surface. All single-wheel nose landing gear parameters are consistent with those in **Table 2**.

Figure 5. Shimmy test setup for the nose landing gear.

Table 2. Parameters and values of the single-wheel nose landing gear shimmy model for the experiment.

Parameters	definition	value	unit
m	Mass of wheel and strut assembly	0.5	Kg
R	Wheel radius	0.05	m
δ	Rake angle	0.157	rad
ζ	Damping ratio	0.5	
H	Landing gear height	0.31	m
L_g	Strut height	0.18	m
d	Strut diameter	0.2	m
I	Moment of inertia of the wheel-strut assembly about the strut axis	1.56×10^{-4}	Kg·m^2
K_s	Lateral bending stiffness of the strut	2.71×10^5	N/m
C_s	Lateral bending damping coefficient of the strut	6.6	N·m·s/rad
K_θ	Torsional stiffness of the strut	1.03×10^5	N·m/rad
C_θ	Torsional damping coefficient of the strut	2.5	N·m·s/rad
K_Δ	Lateral stiffness coefficient of the tire	12,000	N/m
C_Δ	Lateral damping coefficient of the tire	100	N·m·s/rad
K_φ	Torsional stiffness of the tire	700	m/rad
C_φ	Torsional damping coefficient of the tire	0.8	N·m·s/rad
V	Speed	0 - 50	m/s

Below are the experimentally measured relationship graphs for frequency vs. amplitude, frequency vs. velocity, and frequency vs. acceleration at the corresponding speeds.

The relationship graphs for a speed of $V = 5$ m/s are shown in Figure 6:

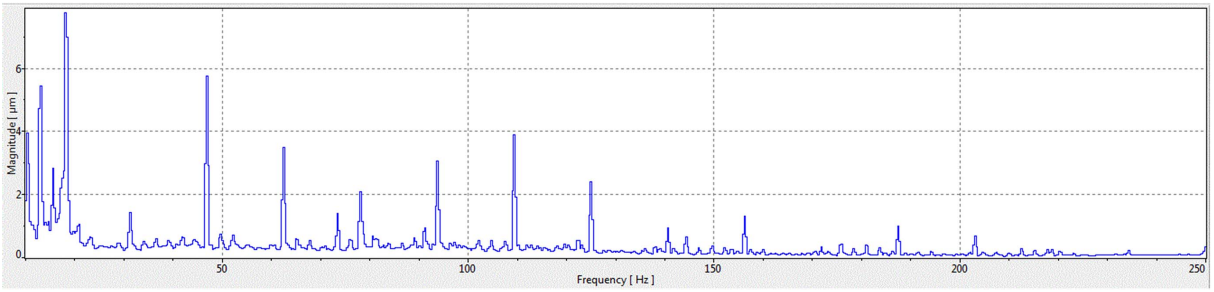

(a)

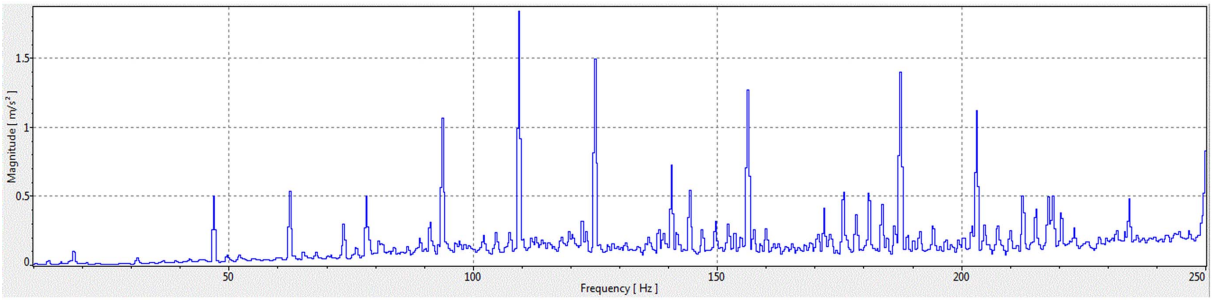

(b)

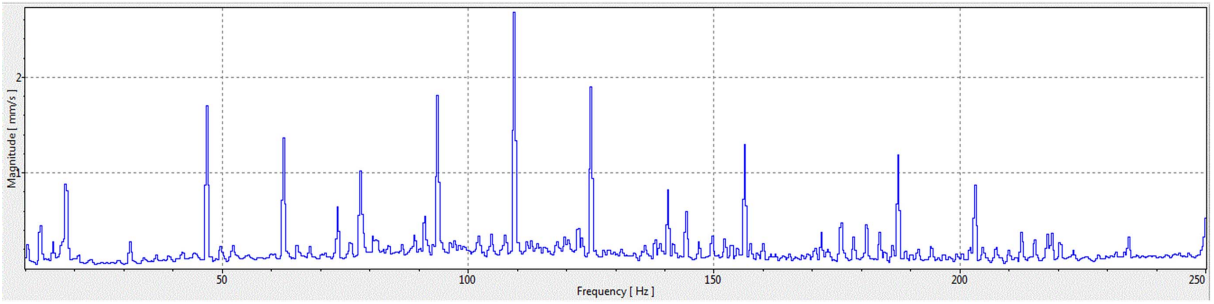

(c)

Figure 6. V = 5 m/s (a) Frequency vs. Amplitude; (b) Frequency vs. Velocity; (c) Frequency vs. Acceleration.

The relationship graphs for a speed of $V = 10$ m/s are shown in Figure 7:

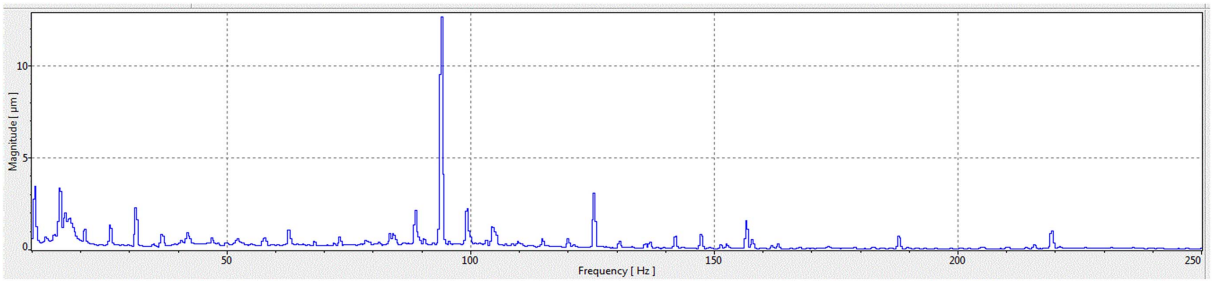

(a)

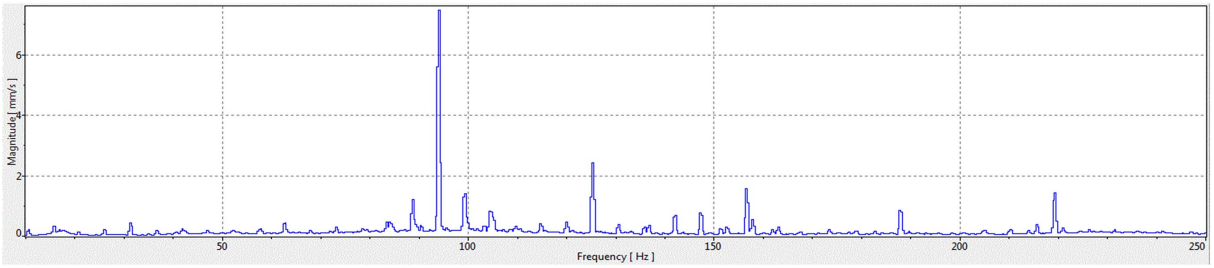

(b)

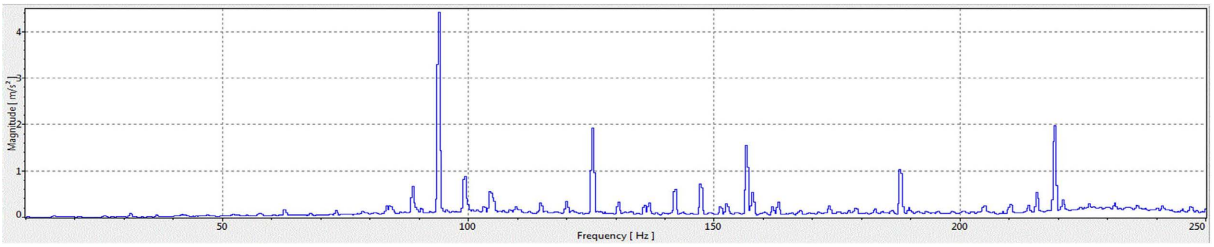

(c)

Figure 7. V = 10 m/s (a) Frequency vs. Amplitude; (b) Frequency vs. Velocity; (c) Frequency vs. Acceleration.

The relationship graphs for a speed of V = 15 m/s are shown in **Figure 8**:

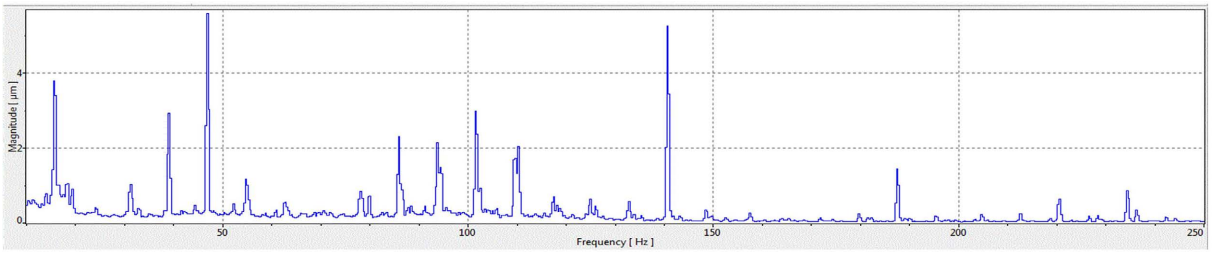

(a)

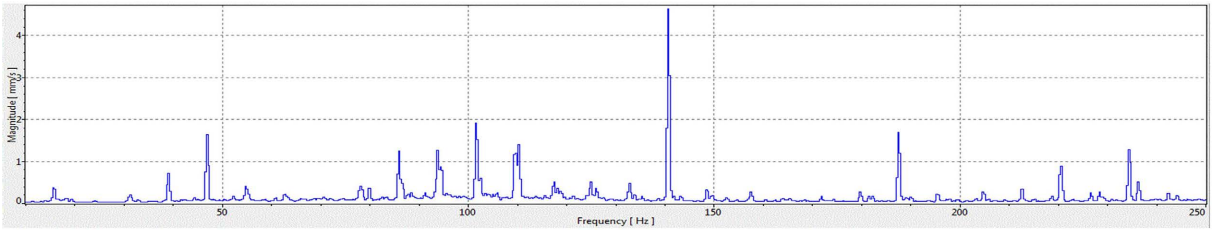

(b)

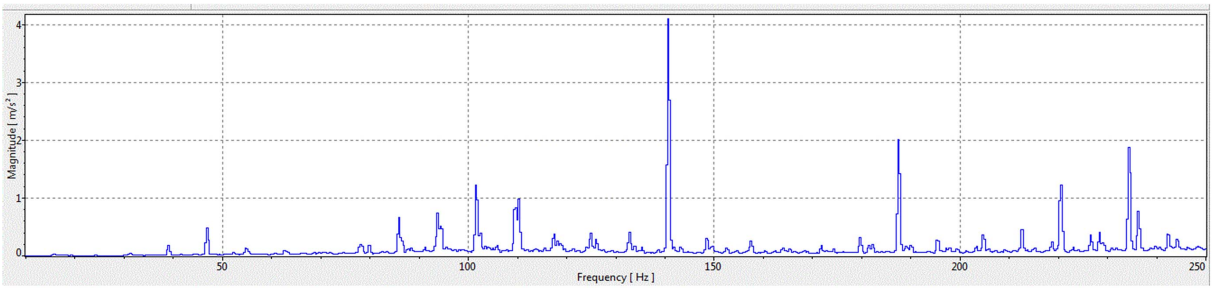

(c)

Figure 8. V = 15 m/s (a) Frequency vs. Amplitude; (b) Frequency vs. Velocity; (c) Frequency vs. Acceleration.

The relationship graphs for a speed of $V = 20$ m/s are shown in **Figure 9**:

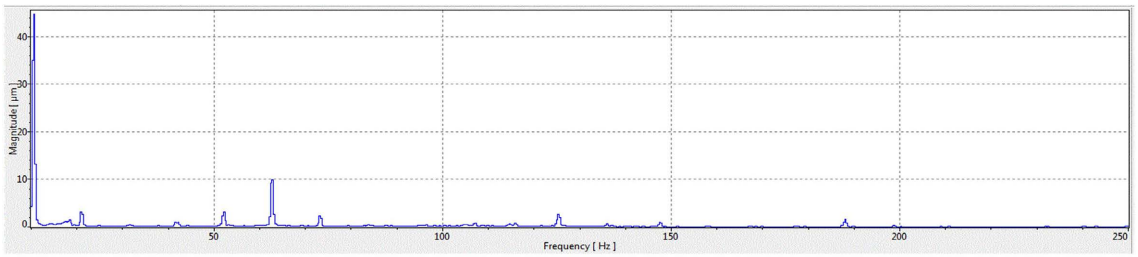

(a)

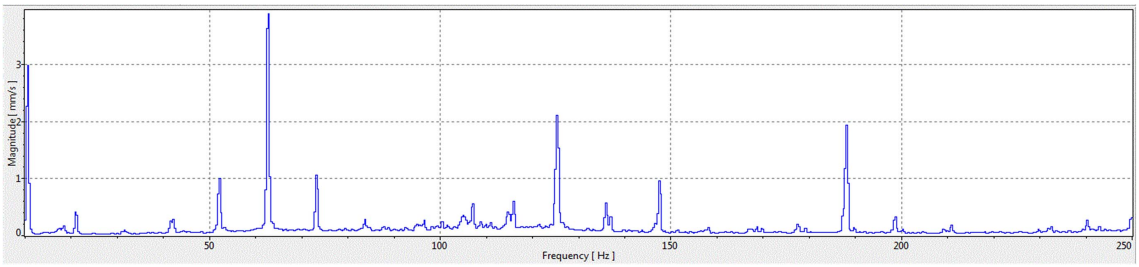

(b)

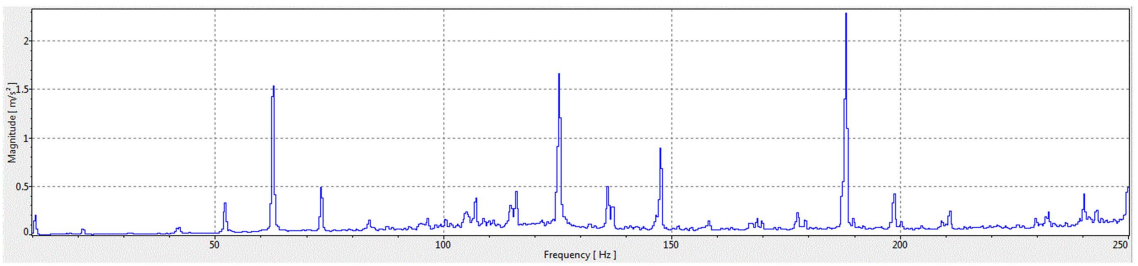

(c)

Figure 9. V = 20 m/s (a) Frequency vs. Amplitude; (b) Frequency vs. Velocity; (c) Frequency vs. Acceleration.

The relationship graphs for a speed of $V = 25$ m/s are shown in **Figure 10**:

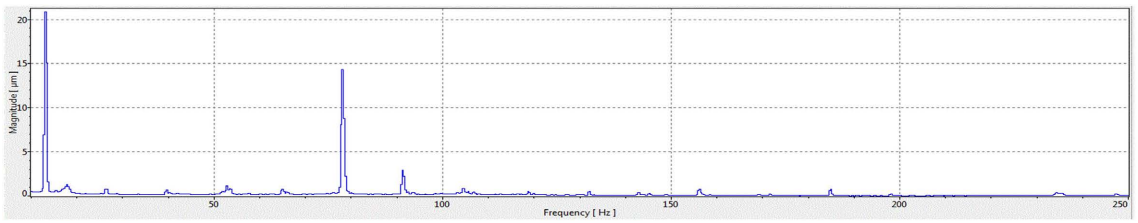

(a)

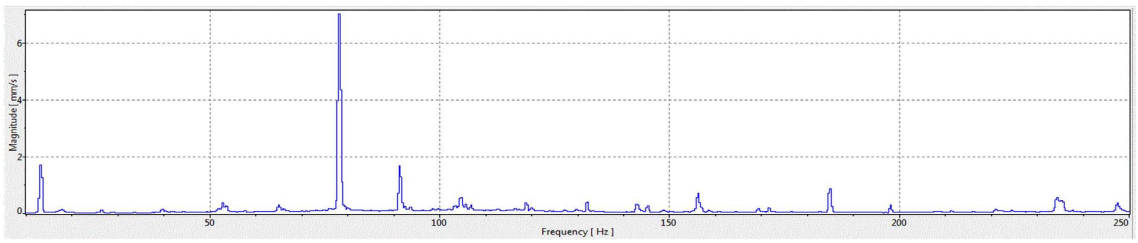

(b)

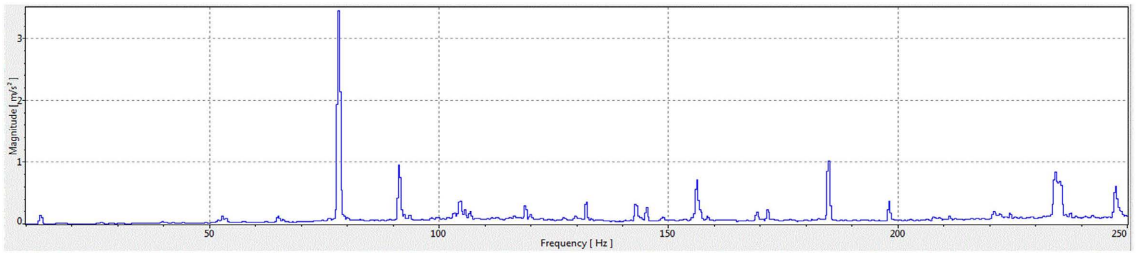

(c)

Figure 10. V = 25 m/s (a) Frequency vs. Amplitude; (b) Frequency vs. Velocity; (c) Frequency vs. Acceleration.

The relationship graphs for a speed of $V = 30$ m/s are shown in **Figure 11**:

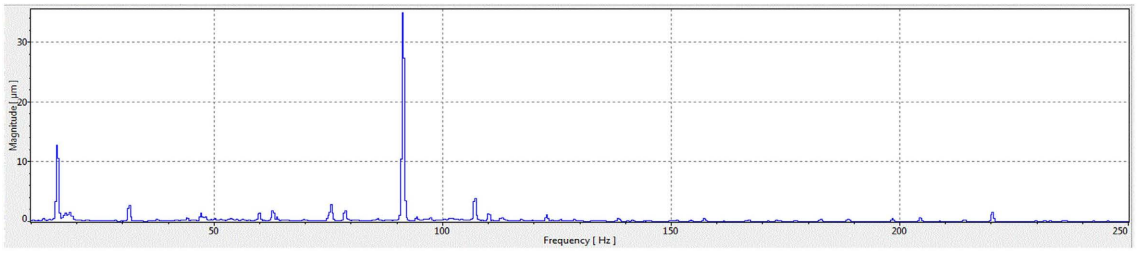

(a)

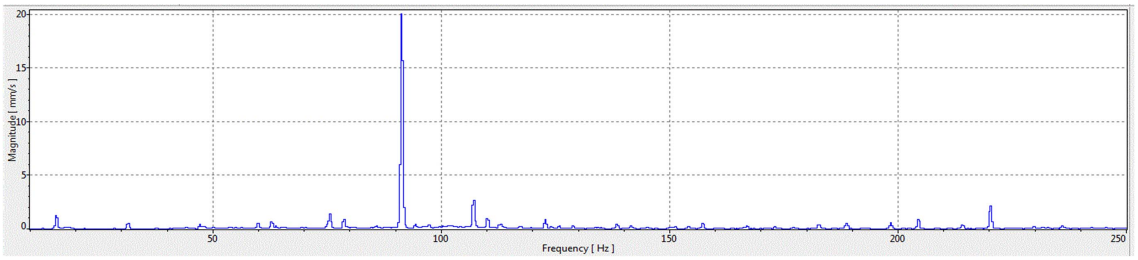

(b)

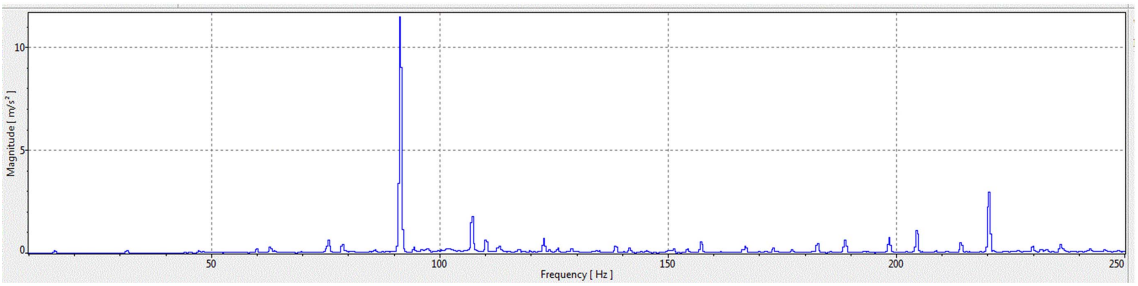

(c)

Figure 11. V = 30 m/s (a) Frequency vs. Amplitude; (b) Frequency vs. Velocity; (c) Frequency vs. Acceleration.

As shown in the figures above, the vibration response of the landing gear tire changes with increasing speed. When the tire's taxiing speed is 20 m/s, the vibration amplitude reaches its maximum value of 42 micrometers, corresponding to a frequency of 2 Hz. When the speed increases to 30 m/s, the vibration frequency rises to 91 Hz, while the amplitude slightly decreases to 34 micrometers. In terms of velocity response, at a taxiing speed of 30 m/s, the peak velocity response

reaches approximately 20 mm/s, occurring at a frequency of 92 Hz. In contrast, at a speed of 25 m/s and a frequency of 78 Hz, the peak velocity response is only 8 mm/s. The acceleration response shows more pronounced changes, reaching a maximum value of 12 m/s^2 at a taxiing speed of 30 m/s, with the peak corresponding to a frequency of 91 Hz. At 25 m/s and a frequency of 78 Hz, the acceleration response is 3.4 m/s^2.

Further comparison of **Figure 6**, **Figure 9**, and **Figure 11** reveals that as the taxiing speed increases, the growth trends of the vibration parameters become evident:

1) **Amplitude Variation:** Compared to the low speed of 5 m/s, when the taxiing speed increases to 20 m/s, the amplitude expands from 7 micrometers to 42 micrometers, a 6-fold increase. When the speed further increases to 30 m/s, the amplitude slightly decreases but remains at a relatively high level. This indicates that the amplitude initially increases with speed within a certain range, reaches a peak, and then begins to decrease.

2) **Velocity Response:** At a taxiing speed of 5 m/s, the velocity response is 2.6 mm/s, while at 30 m/s, the peak velocity response reaches 20 mm/s, an increase of approximately 9 times. The experimental data show that the velocity response exhibits a more significant increase trend at high taxiing speeds.

3) **Acceleration Variation:** At the low speed of 5 m/s, the acceleration response is 1.8 m/s^2, while at 30 m/s, the maximum acceleration increases to 12 m/s^2, a 6.7-fold increase. The acceleration shows a growing trend with increasing taxiing speed, particularly in the high-frequency range.

4.3. Summary of Trends

The experimental results reveal the following characteristics of the landing gear tire's vibration response:

1) The amplitude significantly increases with taxiing speed but begins to decrease after reaching a peak at 20 m/s. The experimental results show that the system's amplitude significantly increases when approaching the critical shimmy speed, which aligns with the theoretically calculated critical shimmy speed range (10 m/s - 20 m/s).

2) Both velocity and acceleration responses increase exponentially with taxiing speed, showing more pronounced peak responses at high speeds. The higher the speed, the higher the peak, indicating that high-frequency vibrations have a greater impact on the system's dynamic performance.

3) Amplitude, velocity response, and acceleration response all exhibit peaks corresponding to specific speeds and frequencies, indicating that the system tends to resonate under certain conditions.

In terms of acceleration alone, it increases with the speed of the landing gear tire. As the speed increases, the vibration frequency corresponding to the acceleration changes also shifts. The graphs show that each experiment exhibits three distinct regions of significant acceleration changes. The higher the speed, the

higher the frequency at which these changes occur, and the acceleration peaks show a clear backward shift.

From this experiment, it is evident that as the landing gear system is driven by the flywheel, the tire gains speed. When the speed increases from 10 m/s to 20 m/s, the landing gear tends to become unstable, with the amplitude increasing by at least 6 times. However, when the speed increases to 30 m/s, compared to 20 m/s, the frequency at which instability occurs shifts backward to 16 Hz, and the amplitude decreases from 42 micrometers to 32 micrometers, though it remains significantly higher than 7 micrometers. This shows that while an increase in tire speed does not necessarily lead to a larger amplitude and instability in the strut's midsection, it does increase the acceleration.

5. Conclusions

This paper addresses the stability issue of aircraft nose landing gear shimmy by combining theoretical modeling and experimental validation. It systematically analyzes the influence of strut height and structural parameters on the critical shimmy speed and frequency, and proposes optimization design recommendations. The main research content and conclusions are as follows:

1) Theoretical Modeling and Parameter Analysis

A nonlinear dynamic model incorporating strut height and slenderness ratio is developed, revealing that increased strut height weakens lateral bending stiffness and damping.

Analytical expressions for critical shimmy speed and frequency indicate that a higher strut height lowers the critical speed, increasing the likelihood of shimmy instability.

2) Experimental Validation and Time-Domain Response Analysis

Experimental Design: A shimmy test platform for the nose landing gear was constructed, and data were collected using a PSVQTec3D 3D laser vibrometer. Dynamic responses at different taxiing speeds (5 - 30 m/s) were tested.

Key Findings:

Amplitude Characteristics: At a taxiing speed of 20 m/s, the peak amplitude reaches 42 μm (a 6-fold increase compared to 5 m/s), approaching the theoretical critical speed range (10 - 20 m/s).

Acceleration Response: At high speeds (30 m/s), the peak acceleration reaches 12 m/s^2, with the frequency shifting to higher modes (91 Hz).

Stability Boundary: Below the critical speed (67 m/s), the system remains stable with convergent responses; above the critical speed, the responses diverge, validating the accuracy of the theoretical model.

3) Engineering Implications and Future Research

This study provides practical design insights for mitigating shimmy instability in high-strut landing gears, relevant to commercial airliners and transport aircraft.

Future research should explore multi-body dynamics and aeroelastic interactions to develop advanced shimmy suppression strategies, especially for landing

gear systems operating under variable runway conditions.

4) Innovations and Contributions

Experimental Validation: High-precision laser vibrometry quantifies the bifurcation characteristics of shimmy responses with speed, filling the gap in experimental data for high-strut landing gears.

Engineering Value: Provides parameter matching guidelines for anti-shimmy design of landing gears, particularly suitable for wide-body airliners and transport aircraft with high-strut configurations.

5) Future Prospects

Future research could further integrate multi-body dynamics and aeroelastic coupling effects to explore shimmy suppression strategies under complex runway excitations and extend to the cooperative stability analysis of multi-wheel landing gear systems.

By combining theoretical derivation and experimental validation, this paper provides important insights into the mechanism analysis and engineering optimization of aircraft landing gear shimmy issues.

Funding

This work was supported by the National Natural Science Foundation of China (12072140).

Conflicts of Interest

The authors declare no conflicts of interest regarding the publication of this paper.

References

[1] Liu, X.C., Liu, C.C. and Mou, R.K. (2022) Research Progress on Shimmy Dynamics of Aircraft Landing Gear Systems. *Acta Aeronautica et Astronautica Sinica*, **43**, 106-121.

[2] Somieski, G. (1997) Shimmy Analysis of a Simple Aircraft Nose Landing Gear Model Using Different Mathematical Methods. *Aerospace Science and Technology*, **1**, 545-555. https://doi.org/10.1016/s1270-9638(97)90003-1

[3] Liu, S.L., Liu, X.C., Cui, R.R., *et al.* (2017) Study on the Influence of Local Stiffness at the Connection of Aircraft Bodies on the Stability of Landing Gear Swing in Light Aircraft. *Journal of Vibration Engineering*, **30**, 249-254.

[4] Liu, C.C., Liu, S.L. and Cui, R.R. (2017) Analysis of Front Landing Gear Swing Considering the Influence of Local Stiffness of the Aircraft. *Mechanical Science and Technology for Aerospace Engineering*, **36**, 811-815.

[5] Thota, P., Krauskopf, B. and Lowenberg, M. (2010) Bifurcation Analysis of Nose-Landing-Gear Shimmy with Lateral and Longitudinal Bending. *Journal of Aircraft*, **47**, 87-95. https://doi.org/10.2514/1.43507

[6] Thota, P., Krauskopf, B. and Lowenberg, M. (2008) Interaction of Torsion and Lateral Bending in Aircraft Nose Landing Gear Shimmy. *Nonlinear Dynamics*, **57**, 455-467. https://doi.org/10.1007/s11071-008-9455-y

[7] Rahmani, M. and Behdinan, K. (2019) On the Effectiveness of Shimmy Dampers in Stabilizing Nose Landing Gears. *Aerospace Science and Technology*, **91**, 272-286. https://doi.org/10.1016/j.ast.2019.05.040

[8] Zhou, J.X. and Zhu, D.P. (1998) Structural Vibration and Its Influencing Factors. *Strength and Environment*, No. 2, 62-64.

[9] Chen, Y., Cui, R., Ju, R. and Dou, Q. (2018) Simulation of Nose Landing Gear Shimmy with Flexible Airframe Considered. *Xibei Gongye Daxue Xuebao/Journal of Northwestern Polytechnical University*, **36**, 388-395. https://doi.org/10.1051/jnwpu/20183620388

[10] Laporte, D.J., Lopes, V. and Bueno, D.D. (2019) An Approach to Reduce Vibration and Avoid Shimmy on Landing Gears Based on an Adapted Eigenstructure Assignment Theory. *Meccanica*, **55**, 7-17. https://doi.org/10.1007/s11012-019-01101-4

[11] Arreaza, C., Behdinan, K. and Zu, J.W. (2016) Linear Stability Analysis and Dynamic Response of Shimmy Dampers for Main Landing Gears. *Journal of Applied Mechanics*, **83**, Article ID: 081002. https://doi.org/10.1115/1.4033482

[12] Moreland, W.J. (1954) The Story of Shimmy. *Journal of the Aeronautical Sciences*, **21**, 793-808. https://doi.org/10.2514/8.3227

[13] Von Schlippe, B. and Dietrich, R. (1947) Shimmying of a Pneumatic Wheel. NACA TM 1365.

[14] Sura, N.K. and Suryanarayan, S. (2007) Closed Form Analytical Solution for the Shimmy Instability of Nose-Wheel Landing Gears. *Journal of Aircraft*, **44**, 1985-1990. https://doi.org/10.2514/1.28826

[15] Boeckh (1954) Determination of the Elastic Constants of Airplane Tires. Technical Report Archive and Image Library.

[16] Von Schlippe, B. and Dietrich, R. (1954) Shimmying of a Pneumatic Wheel. NACA.

[17] Howcroft, C., Lowenberg, M., Neild, S. and Krauskopf, B. (2013) Effects of Freeplay on Dynamic Stability of an Aircraft Main Landing Gear. *Journal of Aircraft*, **50**, 1908-1922. https://doi.org/10.2514/1.c032316

[18] Rahmani, M. and Behdinan, K. (2020) Interaction of Torque Link Freeplay and Coulomb Friction Nonlinearities in Nose Landing Gear Shimmy Scenarios. *International Journal of Non-Linear Mechanics*, **119**, Article ID: 103338. https://doi.org/10.1016/j.ijnonlinmec.2019.103338

[19] Smiley, R.F. (1957) Correlation, Evaluation, and Extension of Linearized Theories for Tyre Motion and Wheel Shimmy. NACA 1299.

[20] Rahmani, M. and Behdinan, K. (2019) Investigation on the Effect of Coulomb Friction on Nose Landing Gear Shimmy. *Journal of Vibration and Control*, **25**, 255-272. https://doi.org/10.1177/1077546318774440

[21] James, T.G. (2002) Perturbation Analysis of Nonlinear Wheel Shimmy. *Journal of Aircraft*, **39**, 305-317. https://doi.org/10.2514/2.2928

[22] Feng, F., Luo, B., Zhang, C., *et al.* (2019) Analysis of the Influence of Wheel Spacing and Dual Wheel Rotation on Aircraft Landing Gear Swing. *Journal of Vibration and Shock*, **38**, 212-217.

[23] Ruan, S., Zhang, M. and Nie, H. (2024) Analysis of the Influence of Structural Clearance on the Ground Sliding Vibration Characteristics of Landing Gear. *Vibration and Impact*, **43**, 234-243.

[24] Verduzco, F. and Alvarez, J. (2006) Hopf Bifurcation Control: A New Approach. *Systems & Control Letters*, **55**, 437-451. https://doi.org/10.1016/j.sysconle.2005.09.007

[25] Lee, Y.S., Vakakis, A.F., Bergman, L.A. and Michael McFarland, D. (2006) Suppression of Limit Cycle Oscillations in the Van Der Pol Oscillator by Means of Passive Non-Linear Energy Sinks. *Structural Control and Health Monitoring*, **13**, 41-75. https://doi.org/10.1002/stc.143

[26] Besselink, I.J.M. (2000) Shimmy of Aircraft Main Landing Gears. *Mechanical Maritime & Materials Engineering*.

[27] Yi, C., Rongyao, C., Rongbo, J., *et al*. (2018) Simulation of Nose Landing Gear Shimmy with Flexible Airframe Considered. *Journal of Northwestern Polytechnical University*, **36**, 388-395.

[28] Bronkhorst, K.B., Febbo, M., Lopes, E.M.O. and Bavastri, C.A. (2018) Experimental Implementation of an Optimum Viscoelastic Vibration Absorber for Cubic Nonlinear Systems. *Engineering Structures*, **163**, 323-331. https://doi.org/10.1016/j.engstruct.2018.02.074

[29] Ma, R., Bi, K. and Hao, H. (2020) Using Inerter-Based Control Device to Mitigate Heave and Pitch Motions of Semi-Submersible Platform in the Shallow Sea. *Engineering Structures*, **207**, Article ID: 110248. https://doi.org/10.1016/j.engstruct.2020.110248

[30] Qiu, Z. and Wang, T. (2019) Laser Dot Projection Videogrammetry for Vibration Measurement and Control of a Piezoelectric Flexible Cantilever Plate. *Aerospace Science and Technology*, **94**, Article ID: 105397. https://doi.org/10.1016/j.ast.2019.105397